A Thermodynamic Analysis of a Solar-Powered Jet Refrigeration System

F. L. Lansing and V. W. Chai
DSN Engineering Section

The article describes and analyzes a method of using solar energy to drive a jet refrigeration system. A new technique is presented in the form of a performance nomogram combining the energy and momentum equations to determine the performance characteristics. A numerical example, using water as the working fluid, is given to illustrate the nomogram procedure. The resulting coefficient of performance was found comparable with other refrigeration systems such as the solar-absorption system or the solar-Rankine turbocompressor system.

I. Introduction

As part of the Deep Space Network energy conservation project made for the Deep Space Communication Complex (DSCC) at Goldstone, California, many energy-conservation money-saving ideas are being studied to reduce the complex dependence on fossil fuel or electric-powered devices. The existing heating, ventilation, and air-conditioning equipment (HVAC) presents a sizable share of the total energy consumption of the complex, and the concept of utilizing the abundant solar energy falling on the site is under investigation.

The present state-of-the-art of solar-powered cooling devices is still limited to several options. Examples are: (1) a solar-powered Rankine engine driving a vapor compression refrigeration machine, (2) solar-powered photovoltaic array (concentrated on nonconcentrated) driving a vapor compression refrigeration machine, and (3) a solar-powered absorption refrigeration. The first option employs two rotating parts such as turbines (or engines), and compressors (excluding the pump) that have to be specially designed to adapt the low temperature nature of solar energy. The second option, though directly generates electricity with less mechanical parts, is neither economically competitive nor has the same conversion efficiency with the first. The third option possesses the highest coefficient of performance, but has some size, maintenance, and operation difficulties.

One of the least commonly used refrigeration techniques today is the jet refrigeration system (Refs. 1, 2 and 3). This system has not enjoyed wide application despite its advantages of simplicity, ruggedness of design, vibration-free, reliability, and its low operation and maintenance cost. Coupling this system with solar-energy as a driving source instead of conventional gas-fired boilers adds a new option to solar-powered cooling devices. This work intends to introduce the concept, describe the relevant parameters, and present the new analytic methodology used in performance determination.

II. System Description

The basic concept of a solar-powered vapor compression refrigeration system, as illustrated in Fig. 1, is to use a solar-Rankine power cycle to drive a vapor compression refrigeration cycle. Solar energy is used to vaporize the working fluid of the power cycle to saturated vapor at the boiler. Nonconcentrating flat-plate solar collectors or medium-concentration types can be used for this task to provide fluid temperatures that range from 90 to 160°C. For most working fluids, this range of temperatures is sufficient for vaporization. The vapor expands in the turbine and produces the mechanical work that is needed to drive the refrigeration compressor. The combination of the turbine and the compressor on a single shaft is sometimes called a turbo-compressor unit (Ref. 4).

The working fluids and the temperatures used in both cycles so far can be independent of each other. In each cycle, the choice of the working fluid depends on performance, stability, economics, and safety factors.

Figure 2 shows a modified solar-powered vapor compression refrigeration system where both power and refrigeration cycles are employing the same working fluid and have a common condenser. The common condenser acts for both cycles as a heat sink at a uniform temperature. This configuration with a single working fluid has been recommended (Ref. 5) for its compactness and low maintenance cost benefits, though it does not have the choice of many working fluids due to chemical and thermal stability in the combined cycle.

The only role of the turbo-compressor unit (Figs. 1 and 2) is to expand in the turbine the vapor from the boiler pressure down to the condenser pressure and to compress in the compressor the vapor from the evaporator pressure up to the condenser pressure, thus exchanging two equal but opposite mechanical operations. This energy exchange, from thermodynamics viewpoint has a null effect on the overall cycle performance. The same function of the turbocompressor can be replaced and made simply by using the ejector scheme as shown in Figs. 3 and 4. The convergent-divergent nozzle replaces the turbine function in converting the enthalpy drop between the boiler pressure and the evaporation pressure to kinetic energy. In practice, the pressure at the nozzle exit (state 4) is made slightly lower than the evaporator pressure (state 5) to overcome the pressure drop in the line. In the mixing chamber, entrainment with momentum exchange occurs between the vapor with supersonic speed leaving the nozzle and the vapor with subsonic speed leaving the evaporator. The mixture (state 6), still with supersonic velocity, will emerge into the diffuser section where it converts its kinetic energy back into an enthalpy increase, thus raising its pressure to the condenser pressure (state 7). The diffuser replaces the compressor function. The condensate from the condenser (state 1) is divided to two branches; one branch goes to the power cycle loop through the pump (state 2) and the solar collector/boiler section to state (3) as vapor, and the other branch goes to the refrigeration cycle loop through an expansion valve (state 8) to the evaporator.

Figure 5 presents the sequence of events for the jet refrigeration scheme on the pressure-enthalpy diagram. Flow irreversibilities in the nozzle and the diffuser occur through the deviation of the isentropic states (state 4_{isen} and state 7_{isen}) from the actual ones (states 4 and 7).

The jet-refrigeration system has many advantages besides operating without gross moving parts (except for the small circulating pump). It is vibration- and noise-free, relatively simple and inexpensive to manufacture with a well-developed technology of nozzles, diffusers, and heat exchangers. The system is low in operation and maintenance cost and its performance is highly competitive with solar-powered turbo-compressor units and solar powered absorption refrigeration units, as will be shown later.

III. Assumptions and Governing Equations

The adiabatic control volume including the nozzle, the mixing chamber, and the diffuser is shown schematically in Fig. 4. Some assumptions are made in the analysis and are listed as follows:

(1) The velocity of the fluid entering the nozzle (state 3) is negligible.

(2) The velocity of the fluid leaving the evaporator (state 5) is negligible.

(3) The velocity of the fluid leaving the diffuser (state 7) is negligible.

(4) The pressure drop through the heat exchangers, and lines is negligible.

(5) Saturated conditions for states 1, 3, and 5 are assumed.

(6) Expansion and compression processes in the nozzle and the diffuser, respectively, are adiabatic.

(7) Heat exchange processes in the evaporator and the condenser are ideal with no thermal losses by radiation.

According to assumptions 1, 2, and 3, the total and static enthalpy of states 3, 5 and 7, as depicted in Fig. 6, will coincide, i.e.,

$$\left.\begin{aligned} H_3 &= H_{3t} \\ H_5 &= H_{5t} \\ H_7 &= H_{7t} \end{aligned}\right\} \tag{1}$$

Applying the first law of thermodynamics on the control volume of Fig. 4 gives:

$$M_1 H_3 + M_2 H_5 = (M_1 + M_2) H_7 \tag{2}$$

where M_1 is the mass flow rate for the power cycle and M_2 is the mass flow rate for the refrigeration cycle. Defining a mass ratio R as

$$R = \frac{M_1}{M_2} \tag{3}$$

Equation (2) can be rewritten in either one of the following forms:

$$\left.\begin{aligned} R &= \frac{H_7 - H_5}{H_3 - H_7} \\ \left(\frac{R}{R+1}\right) &= \frac{H_7 - H_5}{H_3 - H_5} \end{aligned}\right\} \tag{4}$$

Equation (4) indicates that the total enthalpy H_7 is located between the enthalpies H_3 and H_5 and divides their enthalpy difference $(H_3 - H_5)$ inversely by the ratio R, as shown in Fig. 6. Furthermore, applying the first law of thermodynamics and the irreversibility relationships for the nozzle, gives

$$\frac{V_4^2}{2} = (H_3 - H_4) = (H_3 - H_{4,\,\text{isen}}) \times \eta_n \tag{5}$$

and for the diffuser

$$\frac{V_6^2}{2} = H_7 - H_6 = \frac{1}{\eta_d}\,(H_{7,\,\text{isen}} - H_6) \tag{6}$$

where η_n and η_d are the isentropic efficiencies for the nozzle and the diffuser, respectively.

The momentum equation in the constant pressure mixing chamber alone would give:

$$\left.\begin{aligned} M_1 \cdot V_4 &= (M_1 + M_2) \cdot V_6 \\ \text{or} \qquad \frac{V_6^2}{2} &= \left(\frac{R}{1+R}\right)^2 \cdot \frac{V_4^2}{2} \end{aligned}\right\} \tag{7}$$

The thermodynamic properties of states 1, 3 and 5 are completely determined once the three independent temperatures of the boiler, evaporator, and condenser are given. The solution of the set of Eqs. (4), (5), (6), and (7) requires the use of one of the property diagrams together with the design values of η_n and η_d. Instead of the usual trial and error procedure, a performance nomogram will be introduced to match the operating conditions.

A first manipulation of Eqs, (5), (6) and (7) give the following relationship:

$$(H_{7,\,\text{isen}} - H_6) = \left(\frac{R}{R+1}\right)^2 \cdot \eta_n \cdot \eta_d\,(H_3 - H_{4,\,\text{isen}}) \tag{8}$$

The left-hand side of Eq. (8) represents the ideal compression work needed if the diffuser were replaced by an adiabatic compressor. On the other hand, the enthalpy difference $(H_3 - H_{4,\,\text{isen}})$ represents the ideal expansion work obtained if the nozzle were replaced by an adiabatic expander. The unique turbocompressor coupling effect made by the jet refrigeration scheme is clearly shown by the extra quantity $(R/R+1)^2$ in Eq. (8). The fact that the quantity $(R/R+1)^2$ appears is due to the entrainment phenomenon in the mixing chamber and the momentum exchange.

The overall coefficient of performance (*COP*) for the jet refrigeration system is defined as

$$COP = \frac{\text{refrigeration effect}}{\text{external energy input}} \tag{9}$$

The external energy added to the system (Fig. 3) is composed of both the heating part from state (2) to state (3) and the pump work from state (1) to state (3). Accordingly,

$$COP = \frac{(H_5 - H_1)}{R\,(H_3 - H_1)} \tag{10}$$

IV. Carnot's Cycle Idealization

The maximum coefficient of performance of the jet refrigeration scheme can be determined using Carnot's principles as shown in Fig. 7. The Carnot's power cycle shown works between the boiler temperature (T_B) and the condenser temperature (T_c) as its limits. The Carnot's refrigeration cycle works between the condenser temperature (T_c) and the evaporator temperature (T_E) as its limits. Both cycles exchange exactly the same amount of mechanical work, which can be written either as

$$W = Q_B \left(1 - \frac{T_c}{T_B}\right)$$

or (11)

$$W = Q_E \left(\frac{T_c}{T_E} - 1\right)$$

where Q refers to the amount of heat exchanged as shown in Fig. 7. The maximum coefficient of performance can then be written as

$$(COP)_{max} = \frac{Q_E}{Q_B} = \frac{(T_B - T_c)}{(T_B)} \cdot \frac{(T_E)}{(T_c - T_E)} \qquad (12)$$

Combining Eqs. (10) and (12) together, will give the minimum mass ratio R for a given set of enthalpies (H_1, H_3, and H_5) as

$$R_{min} = \frac{(H_5 - H_1)}{(H_3 - H_1)(COP)_{max}} \qquad (13)$$

V. Performance Nomogram

This is a graphical presentation of the system equations presented in Section III including energy, momentum, and continuity equations. The nomogram is illustrated in Fig. 8 and is made up of four curves, one for each quadrant. Knowing the three independent temperatures of the system (for the boiler, the condenser and the evaporator) together with the fifth assumption of saturated conditions, the thermodynamic properties of states 1, 3 and 5 are completely determined. Curve 1 can be constructed using the ejector energy equation, Eq. (4), to plot the mass ratio R as an ordinate versus H_7 as an abscissa. Equation (4) shows that R ranges from zero (at $H_7 = H_5$) to infinity (at $H_7 = H_3$). The Carnot's principle further limits the mass ratio R to only above or at least equal to R_{min} as given by Eq. (13). Accordingly, curve 1 will be divided to two regions: an upper region (above R_{min}), where the performance does not violate the second law of thermodynamics, and the lower region (below R_{min}), which is forbidden. Combining the energy and momentum Eqs. (4), (5), (6), and (7) to eliminate the mass ratio R, the resulting equation will be in the form

$$H_6 = H_7 - \left(\frac{H_7 - H_5}{H_3 - H_5}\right)^2 \cdot \eta_n \cdot \left[H_3 - H_{4,isen}\right] \qquad (14)$$

The construction of the set of curves (2) can then follow using curve 1 and Eq. (14), with the nozzle efficiency (η_n) as a parameter. Curve (2) is a plot of the enthalpy H_6 versus the mass ratio R as shown in Fig. 8. Starting with a suitable value of H_7 at a given η_n, the value of R is determined graphically from curve 1, or numerically by Eq. (4), and together with Eq. (14) a point can be located on curve 2. The nozzle efficiency can then be varied and the set of curves (2) will be completed.

The above method in constructing curve 2 is found more straightforward in computations than other methods. For example, if the enthalpy H_7 was eliminated from Eqs. (4), (5), (6), and (7) instead of R, the following quadratic equation would be solved for a given value of H_6 instead of Eq. (14),

$$R^2 \left(H_6 - H_3 + \eta_n (H_3 - H_{4,isen})\right) - R (H_3 + H_5 - 2H_6) - (H_5 - H_6) = 0 \qquad (15)$$

The set of curves (3) in Fig. 8, is plotted with H_6 and H_7 as coordinates, using Eq. (6) and one of the property diagrams with the diffuser efficiency (η_d) as a parameter. The nomogram is then completed by drawing a straight line in the fourth quadrant that passes through the origin with a 45-deg slope.

The performance characteristics are now ready to be determined for the given boiler, condenser, and evaporator temperatures and the nozzle and diffuser isentropic efficiencies. The path may start, for example, from point A (Fig. 8) at an arbitrary value of H_7, down to curve (4), horizontally to meet curve (3) at point C at the selected diffuser efficiency, up to meet curve (2) at point D at the selected nozzle efficiency, and horizontally to meet curve (1) at point E. At point E the enthalpy H_7 should match the first value chosen at point A, otherwise the loop is repeated until the solution converges.

VI. Nomogram Case Example

The following is a numerical example selected for a jet refrigeration system using water as the working fluid. The

following five independent input conditions are sufficient to describe the system. Numerically they are assigned as

(1) Boiler temperature 93.33°C (200°F)

(2) Condenser temperature 26.67°C (80°F)

(3) Evaporator temperature 4.44°C (40°F)

(4) Nozzle efficiency 0.80

(5) Diffuser efficiency 0.80

The maximum (COP) is calculated from Eq. (12) as 2.27 and the minimum mass ratio (R_{min}) as 0.414. Curves 1, 2, 3 and 4 are constructed as shown in Fig. 8. The coefficient of performance for the above example converges to 0.465 corresponding to a mass ratio of R of 2.02. Also, from the nomogram, the coefficient of performance drops to 0.289 corresponding to a mass ratio of 3.25 if the nozzle and diffuser efficiencies become 0.7 each. On the other hand, the coefficient of performance increases to 0.618 corresponding to a mass ratio of about 1.52 if the nozzle and diffuser efficiencies become 0.9 each. The above indicates how sensitive the performance is to the quality of manufacturing the nozzle and the diffuser. Also, it shows that the performance is comparable to other heat-powered refrigeration techniques.

VII. Summary and Remarks

The following points can be made from this first phase study of solar-powered jet refrigeration and the given example of performance:

(1) A new technique is presented in the form of a performance nomogram combining energy and momentum equations to describe the performance characteristics.

(2) The coefficient of performance obtained in the cited example with a nozzle efficiency of 0.80 and a diffuser efficiency of 0.80 was 0.465. This compares favorably with about 0.6 for the solar-powered absorption unit and with about 0.5 for solar-powered Rankine driving a vapor-compression refrigerator. The jet refrigeration performance has improved to about 0.62 when the nozzle and diffuser efficiencies increased to 0.90. This means that an improvement of the product efficiency from 0.64 to 0.81 (an increase of 27%) has produced a performance increase of about 50%.

(3) The numerical example given can also be very helpful in sizing a 3-ton refrigeration unit (36,000 Btu/hr) to fit a conventional residence house. Based on the mass flow ratio R of 2.02, the mass flow rates entering the evaporator and the nozzle are 15.84 kg/hr and 32.48 kg/hr, respectively, and the boiler heat rate would be about 23 kwh_t (78,610 Btu/hr). If the local solar radiancy is taken as 0.8 kw_t/m^2 (~254 Btu/hr-ft^2), the collector area needed at 45% collector efficiency would be about 64 m^2 (~690 ft^2); an area that is adequate for most south-facing roofs. The ejector unit itself for this type of flow conditions does not exceed 50 cm in length according to manufacturer's specifications.

(4) Performance optimization studies are underway to analyze the effects of different types of working fluids, or the effects of different operating temperatures for the solar collector/boiler, condenser and evaporator. These will be reported later as a second phase of the program.

Definition of Terms

COP	Coefficient of performance
COP_{max}	Maximum coefficient of performance
H	Enthalpy
M_1	Mass flow rate for the power cycle
M_2	Mass flow rate for the refrigeration cycle
R	Mass flow ratio
R_{min}	Minimum flow ratio by Carnot principle
T	Temperature
V	Velocity
η	Efficiency
Subscripts	
B	Boiler
c	Condenser
d	Diffuser
E	Evaporator
n	Nozzle
t	Total (stagnation)
isen	Isentropic

References

1. Anderson, H., "Assessment of Solar Powered Vapor Jet Air-conditioning Systems," presented at 1975 International Solar Energy Congress and Exposition (ISES) held at UCLA, Los Angeles, California, p. 408.
2. Threlkeld, J. L., *Thermal Environmental Engineering*, Sect. 6. Prentice-Hall, Inc., New Jersey, 1962.
3. *ASHRAE Guide and Data Book,* "Steam Jet Refrigeration Equipment," Chap. 12, pp. 133-138, 1967.
4. Barber, R. E., "Solar-air Conditioning Systems Using Rankine Power Cycles – Design and Test Results of Prototype Three-ton Unit," in *Proceedings of the Institute of Environmental Science,* Vol. 1, pp. 170-179, 1975.
5. Biancardi, F. R., et al., "Design and Operation of a Solar-powered Turbocompressor Air-conditioning and Heating System," in *IECEC '75 Record*, pp. 186-194.

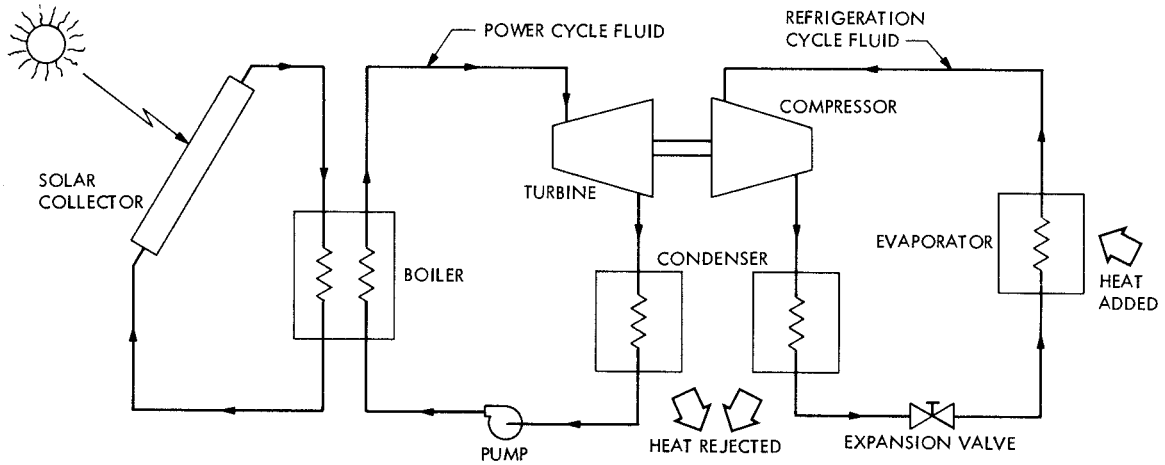

Fig. 1. Double fluid turbocompressor system

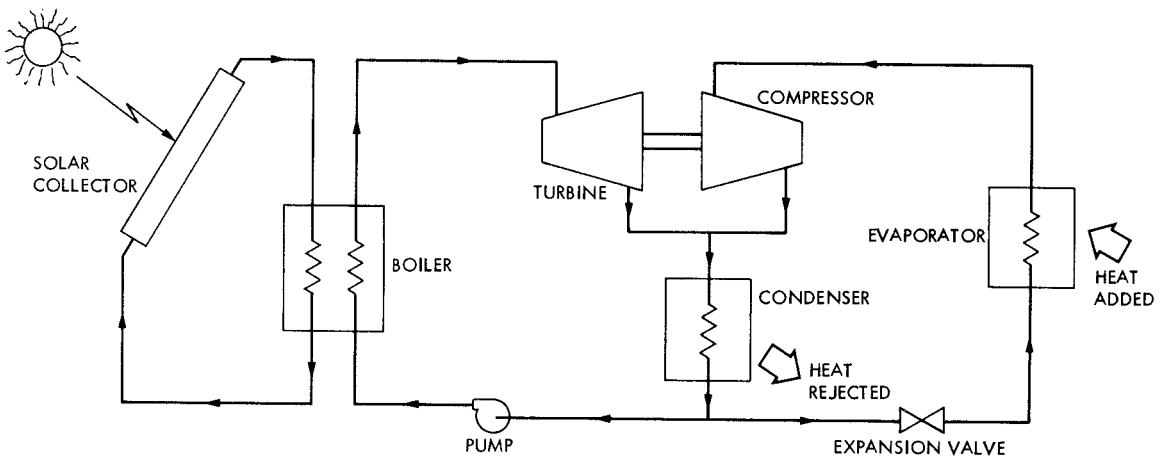

Fig. 2. Single fluid turbocompressor system

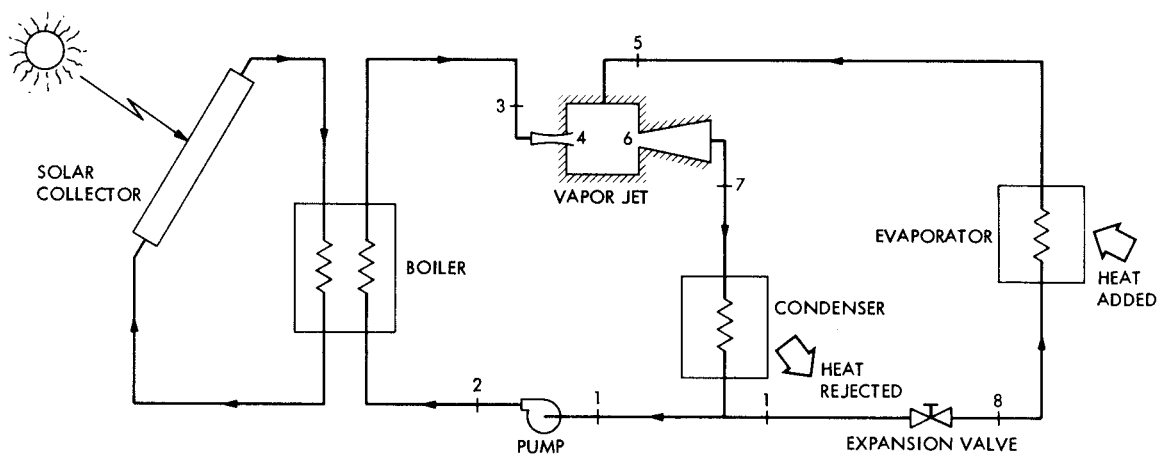

Fig. 3. Vapor jet refrigeration system

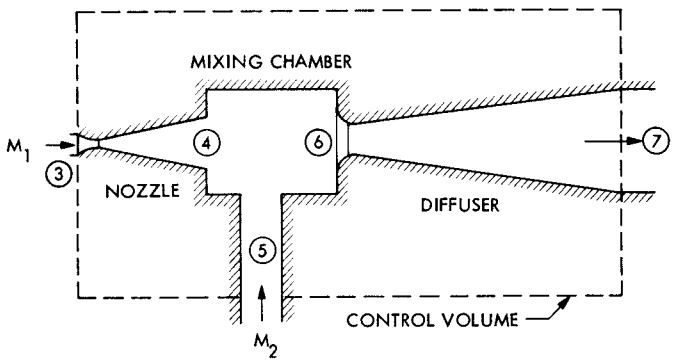

Fig. 4. Ejector control volume

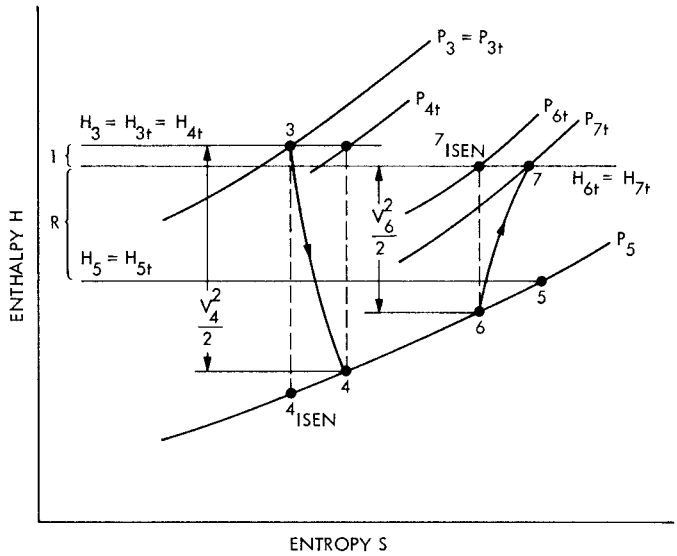

Fig. 6. Ejector presentation on the enthalpy-entropy (Mollier) diagram

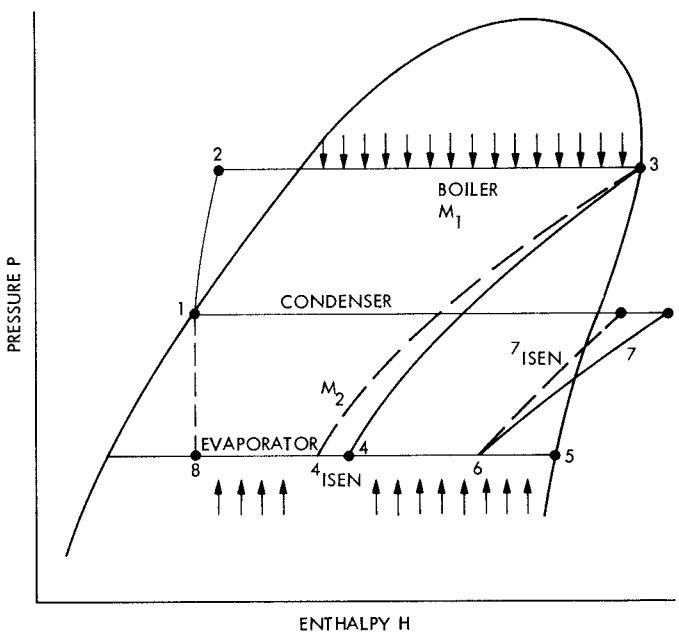

Fig. 5. Pressure-enthalpy diagram showing the complete jet refrigeration cycle

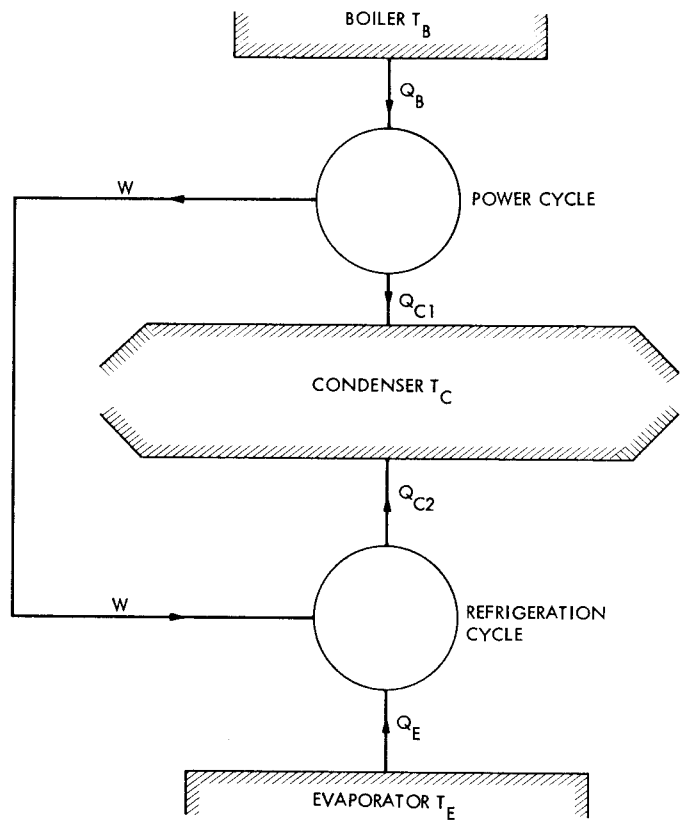

Fig. 7. Carnot cycle idealization for the jet refrigeration scheme

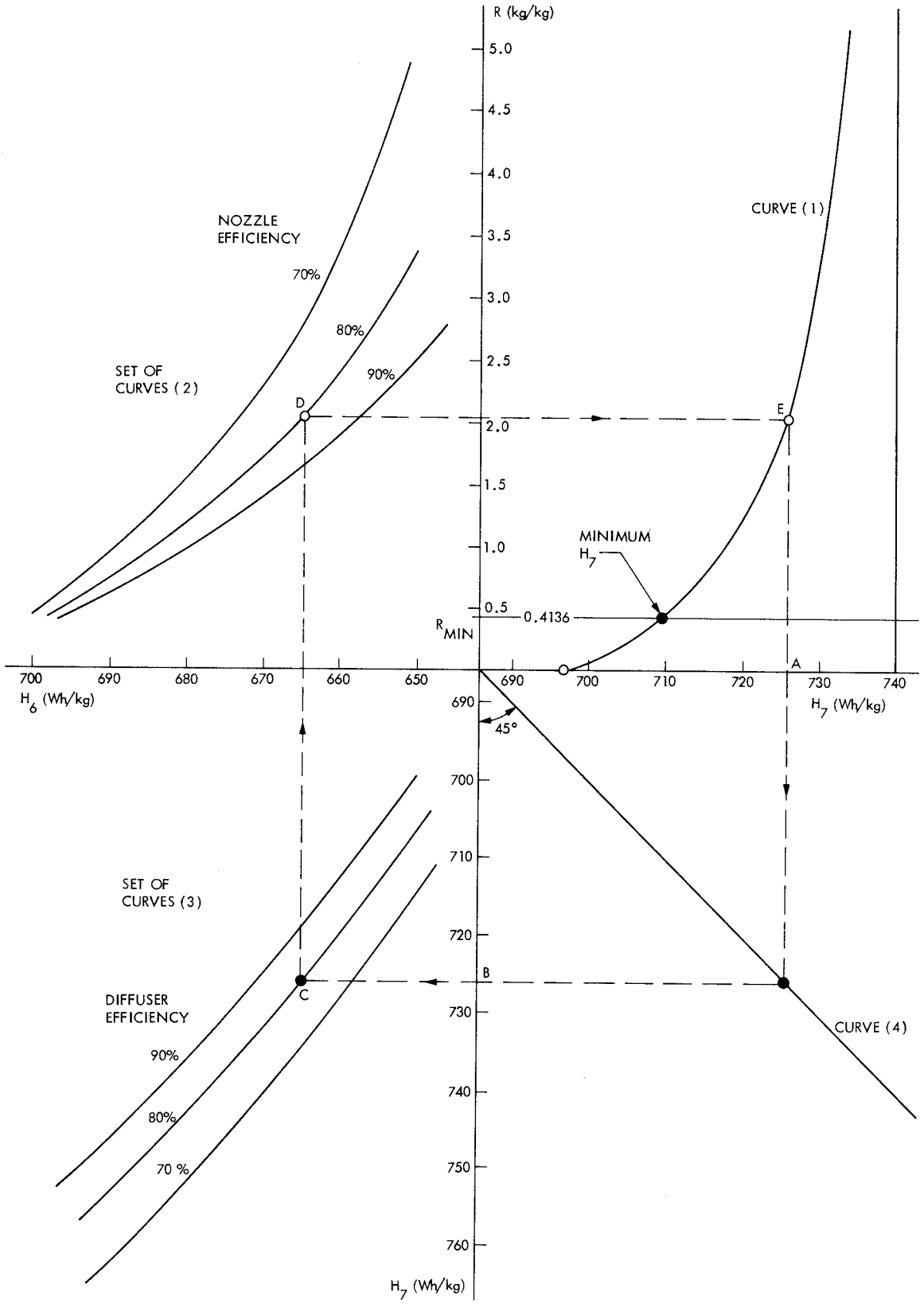

Fig. 8. Performance nomogram for the given operating conditions